Journal of Microscopy, Vol. 209, Pt 1 January 2003, pp. 13–22
Received 15 July 2002; accepted 23 October 2002

Quantitative polarized light microscopy

F. MASSOUMIAN, R. JUŠKAITIS, M. A. A. NEIL & T. WILSON
Department of Engineering Science, University of Oxford, Parks Road, Oxford OX1 3PJ, UK

Key words. Confocal, polarized light microscopy.

Summary

We describe a simple modification to a confocal microscope, which analyses the state of polarization of light emerging from the specimen so as to permit quantitative polarized light microscopy to be performed. The system uses a novel form of rotating analyser which, together with lock-in detection, permits images to be obtained where the image contrast corresponds to both specimen retardance and orientation (e.g. in the case of a birefringent specimen). Images are presented from a wide range of specimens and the origin of the contrast observed from simple point scatterers is investigated both theoretically and experimentally.

Introduction

The state of polarization of a light beam is generally modified when it is reflected from or transmitted through a material. The resulting change in polarization state carries information about the structure of the material. This contrast is used routinely in polarized light microscopy to provide information about specimen birefringence and dichroism in fields as diverse as materials science, crystallography and biology (Gay, 1967; Inoué, 1986; Robinson & Bradbury, 1992). In its simplest form, a conventional or confocal microscope may be converted into a polarization-sensitive instrument merely by inserting a polar into the illumination path and a suitably orientated analyser into the reflected (or transmitted) path. The analyser is orientated so as to pass only light whose polarization is orthogonal to that of the probe beam.

In order to enhance the contrast in polarized light microscopy it is important to reduce to a minimum the contribution to the image which arises from non-scattered light. It is usual to characterize this by an extinction ratio, which is defined as the ratio of light intensity transmitted between parallel polars to that transmitted when the polars are crossed (Pluta, 1993). The measurements are taken in the absence of an object in transmission or in the presence of a perfect reflector in reflection. Ideally, one would like the extinction coefficient to be infinite. However, it is a fundamental consequence of the image formation properties of a conventional microscope that the extinction coefficient is finite even if perfect polars are used (Kubota & Inoué, 1959; Wilson & Juškaitis, 1995) and typically a value of 10^3 is obtained. The coherent image formation in the confocal scanning microscope (Wilson & Sheppard, 1984; Wilson, 1990), on the other hand, permits, in principle, an infinite extinction coefficient to be obtained (Wilson & Juškaitis, 1995). In practice we have obtained values as high as 5×10^5, which was close to the extinction value of our polarizing elements alone. This suggests that the confocal microscope system has an advantage over the conventional in terms of image contrast in polarized light microscopy. However, a drawback with all these instruments is that they provide essentially qualitative information. They do not readily provide quantitative measurements of the spatial distribution of the optical anisotropy of the specimen. In order to overcome this shortcoming we here describe a simple modification to the optical system of a confocal microscope which analyses the polarization state of the image light. This permits images to be obtained which show the spatial variation of the optical retardance and orientation together with a standard confocal image (e.g. in the case of a birefringent sample). These data are acquired with no compromise in the image acquisition rate.

Our approach is to launch circularly polarized light into the microscope optical system and then to detect the image signal at each picture point through a rotating analyser. The speed of rotation of the analyser is sufficiently fast that, together with lock-in detection, demodulated signals containing the retardance, orientation and confocal image intensities may be extracted at each picture point without compromising the image acquisition rate. We will begin by discussing the basis of our method in some detail before describing an electro-optic implementation of the rotating analyser element and finally presenting images of birefringent, dichroic and scattering specimens.

Design outline

The optical system of our polarization contrast microscope is identical to that of a scanning confocal microscope but with the addition of a quarter wave plate on the illumination side

Correspondence to: Prof. T. Wilson. Fax: +44 (0)1865 273905; e-mail: tony.wilson@eng.ox.ac.uk

and a rotating analyser in the detection arm. In order to understand the operation of the system we will concentrate on the case of a linearly birefringent specimen. The Jones matrix for this specimen, which is essentially a linear retarder, may be written (Azzam & Bashara, 1989):

$$T(\delta) = \begin{pmatrix} \exp(j\delta/2) & 0 \\ 0 & \exp(-j\delta/2) \end{pmatrix} \quad (1)$$

where δ represents the relative phase difference (retardance) between light propagating along the two principal axes. In general, of course, the principal axes will be orientated at an angle θ to a fixed set of axes in the optical system and hence the overall Jones matrix may be written as:

$$E = R(-\theta)\,T(\delta)\,R(\theta)\,E_0 \quad (2)$$

where $R(\theta)$ represents the rotation matrix, E_0 is the input field and E represents the output field. If we multiply these matrices together we obtain:

$$\begin{pmatrix} E_x \\ E_y \end{pmatrix} = \begin{pmatrix} \cos(\delta/2) + j\cos(2\theta)\sin(\delta/2) & j\sin(2\theta)\sin(\delta/2) \\ j\sin(2\theta)\sin(\delta/2) & \cos(\delta/2) - j\cos(2\theta)\sin(\delta/2) \end{pmatrix} \begin{pmatrix} E_{x0} \\ E_{y0} \end{pmatrix} \quad (3)$$

It is common in traditional polarized light microscopy to illuminate the specimen with, for example, light polarized in the x-direction

$$\begin{pmatrix} E_{x0} \\ E_{y0} \end{pmatrix} = \begin{pmatrix} 1 \\ 0 \end{pmatrix} E_0$$

and to form an image using the y-polarized component of the image field. Throughout the following we will assume unit amplitude illumination, $E_0 = 1$. This gives an image intensity of the form:

$$I = \sin^2(2\theta)\,\sin^2(\delta/2) \quad (4)$$

The standard technique to measure the orientation θ and the retardance δ is to physically rotate the specimen stage until a null signal is obtained, i.e. to set $\sin^2(2\theta) = 0$. The specimen is then rotated back by 45° so that $\sin^2(2\theta) = 1$ and the value of the retardance is then extracted by tuning a compensator so as to achieve another null signal, $\sin^2(\delta/2) = 0$. As our intention is to extract this information at each picture point this approach is clearly impractical. Instead we choose to illuminate the specimen with circularly polarized light and detect the image signal through an analyser orientated at an angle γ to the x-axis.

If the Jones vector of the illumination is, for example, right circularly polarized,

$$\begin{pmatrix} E_{x0} \\ E_{y0} \end{pmatrix} = \begin{pmatrix} 1 \\ j \end{pmatrix}$$

the transmitted intensity may be written as:

$$I = |E_x \cos\gamma + E_y \sin\gamma|^2 = 1 + \sin(\delta)\sin^2(\gamma - \theta) \quad (5)$$

Because our intention is to extract, at each picture point, δ and θ from this, we elect to rotate the analyser such the angle γ becomes a function of time, $\gamma = \omega_1 t$, and hence the measured intensity also becomes a function of time:

$$I(t) = 1 + \sin(\delta)\,\sin^2(\omega_1 t - \theta) \quad (6)$$

It is now a straightforward matter to use lock-in detection (synchronous demodulation) at a frequency of $2\omega_1$ to obtain two quadrature signals corresponding to $\sin(\delta)\sin(2\theta)$ and $\sin(\delta)\cos(2\theta)$, from which the retardance $|\sin\delta|$ and the orientation θ may be obtained. We perform this operation at each picture point in the image and hence obtain a spatial map of the variation in both the retardance and orientation across the specimen.

Because the image contrast is dependent on the overall polarization change throughout the optical system we elect to use an analyser which behaves as required by Eq. (4) but with no moving parts. We note that Glazer *et al.* (1996) and Oldenbourg & Mei (1995) also use rotating analysers in their widefield microscope implemented as a physically rotating element and by the use of liquid crystal devices, respectively. By contrast, we achieve this using electro-optic phase-shifting element. This approach is advantageous because it allows fast modulation, which is compatible with point-scanning systems (confocal microscopes). As the electro-optic element (Pockels cell) is essentially a linear retarder with an electrically controllable retardance its Jones matrix may be described by Eq. (3) but with an electronically controllable phase difference, ϕ. It is clear from Eq. (3) that if we orientate the electro-optic element such that the direction of its principal axes correspond to $\theta = \pi/4$ then the Jones matrix representing transmission through the Pockels cell itself is given by:

$$T(\phi) = \begin{pmatrix} \cos(\phi/2) & j\sin(\phi/2) \\ j\sin(\phi/2) & \cos(\phi/2) \end{pmatrix} \quad (7)$$

from which it is clear that, together with a quarter wave plate and linear analyser, the overall Jones matrix becomes:

$$\begin{pmatrix} 1 & 0 \\ 0 & 0 \end{pmatrix} \begin{pmatrix} \cos(\phi/2) & j\sin(\phi/2) \\ j\sin(\phi/2) & \cos(\phi/2) \end{pmatrix} \begin{pmatrix} 1 & 0 \\ 0 & -j \end{pmatrix} = \begin{pmatrix} \cos(\phi/2) & \sin(\phi/2) \\ 0 & 0 \end{pmatrix} \quad (8)$$

and hence if a field

$$\begin{pmatrix} E_x \\ E_y \end{pmatrix}$$

were incident on the combination then the intensity of the transmitted light would be given by:

$$I = |E_x \cos(\phi/2) + E_y \sin(\phi/2)|^2 \quad (9)$$

which is, of course, equivalent to Eq. (5) and represents the intensity passed by an analyser at an angle $\gamma = \phi/2$ to the x-axis. Thus, if we apply a suitable voltage ramp to the Pockels cell such that $\phi = \omega t$, then the transmitted intensity is given, by analogy with Eq. (6), as:

$$I(t) = 1 + \sin(\delta)\sin(\omega t - 2\theta) \tag{10}$$

and hence lock-in demodulation at a frequency ω permits us to extract the retardance $|\sin\delta|$ and orientation θ. We shall return to the details of this later.

We have, of course, only considered linear birefringence in the above. It is perfectly straightforward to include the effects of linear dichroism and, indeed, the system permits us to image both the retardance and the dichroism independently. In order to demonstrate this we re-write Eq. (1) as:

$$T(\alpha,\delta) = \begin{pmatrix} \exp\left(\dfrac{\alpha + j\delta}{2}\right) & 0 \\ 0 & \exp\left(-\dfrac{\alpha + j\delta}{2}\right) \end{pmatrix} \tag{11}$$

where α represents the dichroism. If we now choose to illuminate with circularly polarized light

$$\begin{pmatrix} E_{x0} \\ E_{y0} \end{pmatrix} = \begin{pmatrix} 1 \\ \pm j \end{pmatrix}$$

where the positive sign denotes right circular polarization and the minus sign denotes left circular polarization, then the transmitted intensity, measured through a polar orientated at an angle $\phi/2 = \omega t/2$ to the x-axis, is given by:

$$I(t) = \cos h(\alpha) \pm \sin(\delta)\sin(\omega t - 2\theta) + \sin h(\alpha)\cos(\omega t - 2\theta) \tag{12}$$

and hence, by taking images with both left and right circularly polarized input light we may separate the specimen birefringence from the dichroism.

We now complete this section by making some general statements about the way in which the rotating analyser and lock-in detection present the information about the polarization state of the optical field which is incident upon it. Let us assume that this field may be written

$$\begin{pmatrix} E_{x0} \\ E_{y0} \end{pmatrix} = \begin{pmatrix} A \\ B\exp j\Delta \end{pmatrix}$$

where A and B represent the amplitudes of the x and y components, respectively, and Δ denotes their relative phase. This is, of course, an elliptically polarized wave whose polarization state may be conveniently represented by the standard ellipse in Fig. 1. The angle ψ is given by (Born & Wolf, 1975):

$$\tan(2\psi) = \frac{2AB}{A^2 - B^2}\cos(\Delta) \tag{13}$$

When this input field is presented to an analyser orientated at an angle $\phi/2 = \omega t/2$ to the x-axis, the transmitted intensity is given by:

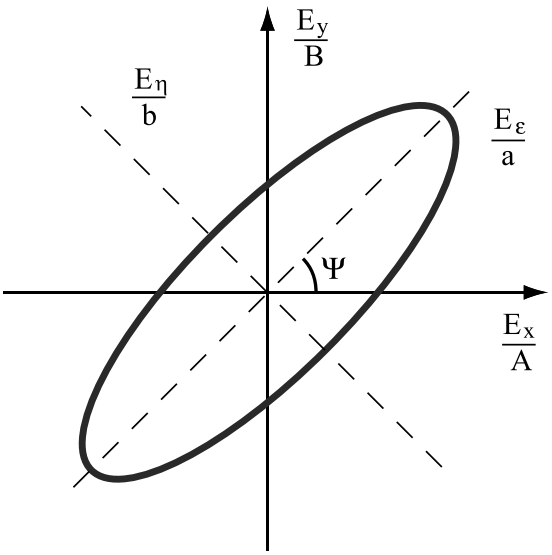

Fig. 1. The polarization ellipse indicating the general state of polarization of an arbitrary input beam. The length of major and minor axes of the ellipse with respect to its principal axes are 2a and 2b, respectively.

$$I(t) = A^2 + B^2 + \sqrt{(A^2 + B^2)^2 + (2AB\cos\Delta)^2}\,\cos(\omega t - 2\psi) \tag{14}$$

If we now rotate the axes such that the polarization ellipse is given, with respect to its principal axes (ξ,η), by:

$$\left(\frac{E_\xi}{a}\right)^2 + \left(\frac{E_\eta}{b}\right)^2 = 1 \tag{15}$$

it is now a straightforward piece of geometry to rewrite Eq. (14) in terms of the amplitudes a and b as:

$$I(t) = a^2 + b^2 + (a^2 - b^2)\cos(\omega t - 2\Psi) \tag{16}$$

The form of Eq. (16) indicates that the images corresponding to three image terms may be extracted using lock-in detection. The first corresponds to $a^2 + b^2$, which represents the intensity of the input field. In terms of microscope imaging, this is equivalent to a normal confocal image. The other two images correspond to the orientation via ψ and the optical anisotropy via $|a^2 - b^2|$. In principle, these data can be made available simultaneously without compromising the image acquisition speed of the confocal microscope.

The experimental system

Figure 2 shows a schematic of the optical system showing the relatively minor modifications required to the usual confocal geometry. A stage scanning approach is preferred in this polarization-sensitive application so as to minimize polarization artefacts due to beam scanning. We note that the same

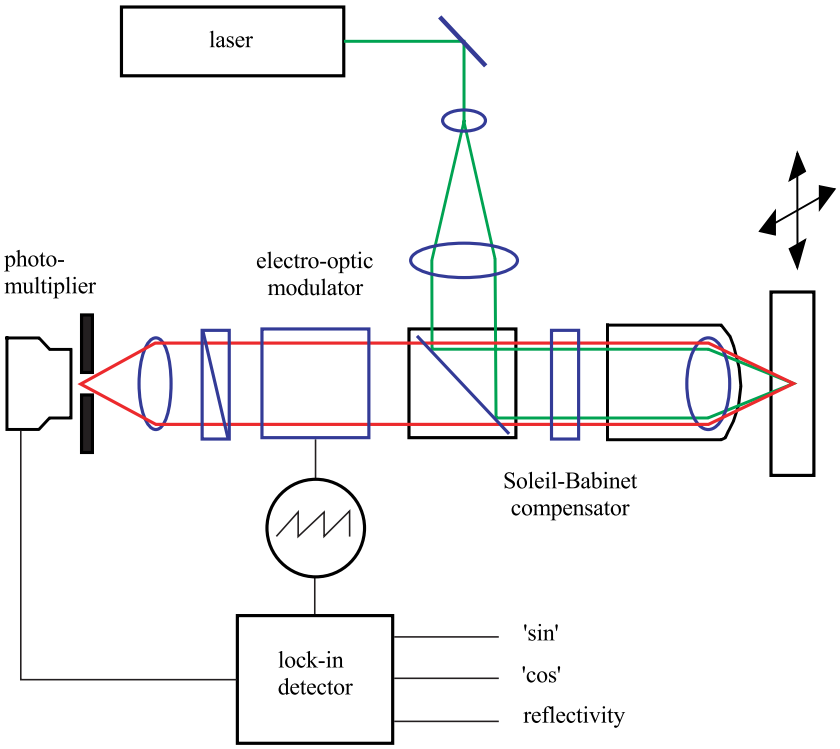

Fig. 2. Schematic diagram of the optical configuration of the polarization contrast confocal microscope. The Soleil-Babinet compensator, set to act as a quarter wave plate, is used both to launch circularly polarized light into the optical system and also as the first element in the electro-optic rotating analyser. The lock-in amplifier detects the two quadrature components from which the magnitude of the optical anisotropy as well as the orientation can be extracted.

quarter wave plate (implemented as a Soleil-Babinet compensator, Melles Griot, UK) is used both to launch circularly polarized light into the microscope as well as to provide the first optical element of the electro-optic rotating analyser. In order to obtain the polarization contrast images a saw-tooth waveform of approximately 200 kHz is generated and used both to ramp the retardance of the Pockels cell and to provide the reference waveforms for the lock-in detection.

Because the rotating analyser is the key element of the system it is important to demonstrate its operation. We do this with the aid of Eq. (8), which predicts that if we sweep the phase such that $\phi = \omega t$ then the transmitted intensity will be of the form $\cos^2(\omega t/2)$ if horizontally polarized light is incident ($E_y = 0$) and similarly the intensity will follow a $\sin^2(\omega t/2)$ function if vertically polarized ($E_x = 0$) light is incident. This behaviour is confirmed experimentally in Fig. 3 where we show the intensity transmitted through the rotating analyser as a function of time for both these input polarization states, together with the saw-tooth waveform which controls the retardance of the Pockels cell. The ADP (ammonium dihydrogen phosphate) Pockels cell, PC100 (Electro Optic Developments Ltd, UK), had a half wave voltage, $V_\pi = 250$ V and a 2 mm square aperture and was 111 mm long.

The system was initially set up with an aluminium mirror as specimen. The Soleil- Babinet compensator was adjusted so that the polarization of the light reaching the modulator was linear, i.e. the demodulated signals were zero. This removed any residual anisotropy still present in the system caused by, for example, imperfections of the non-polarizing beamspitter

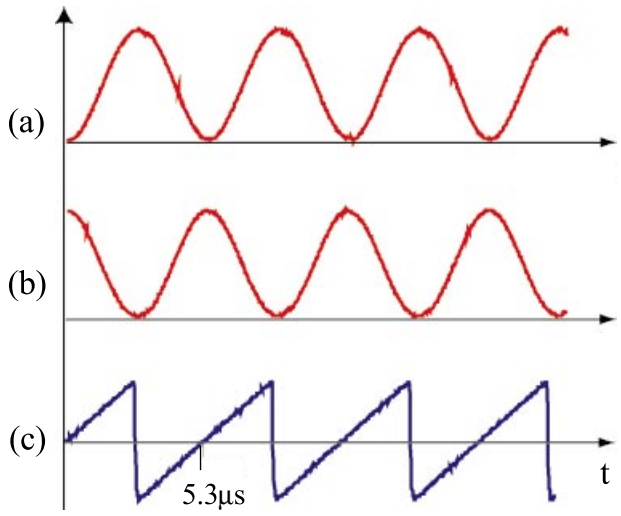

Fig. 3. Experimental confirmation of the operation of the electro-optic implementation of the rotating analyser. The lower trace (c) shows the saw-tooth waveform which is used to sweep the retardance of the Pockels cell. The upper two traces show the measured intensity transmitted when the incident light is (a) vertically and (b) horizontally polarized.

or the objective lens. The noise level, which was dominated by electrical noise in the detection and demodulation circuits, was then measured and calculated to correspond to an equivalent retardance of 1.4 $pm/\sqrt{\text{Hz}}$. Typical pixel dwell times in our system were of the order of 100 ms but, of course, this may be varied according to the sensitivity requirements.

Because the lock-in detection system was required to operate at 200 kHz we elected to construct the circuit from readily available discrete components and to demodulate so as to obtain both quadrature components. In terms of a general polarization state this results, when demodulating with cos (ωt), in a signal of the form:

$$I_c = (a^2 - b^2)\cos(2\Psi) \tag{17}$$

whereas deomdulating with sin (ωt) leads to:

$$I_s = (a^2 - b^2)\sin(2\Psi) \tag{18}$$

It is then a simple matter to extract the magnitude and orientation images from these two raw demodulated signals. We note that the confocal signal ($a^2 + b^2$) is also available simultaneously.

In the next section we present images obtained with this system and, in order to encode the state of polarization in as simple a manner as possible, we elect to use the colour map of Fig. 4. In this figure the direction of the arrow denotes the orientation of the principal axis of the ellipse via the hue of the colour, whereas the saturation, radial distance, denotes the ellipticity. The same colour coding scheme is used in all the figures.

Examples of images

We will begin our discussion of the imaging capabilities of our system by presenting reflection images obtained at room temperature from the superconducting crystal $Y_1Ba_2Cu_3O_{6.94}$, which is of interest because this superconductor possesses one of the highest critical temperatures, $T_c = 92.4$ K. Although it is inappropriate here to discuss the material properties in detail it will suffice to say that it can grow in domain structures and that, within a domain, the structure is somewhat akin to a fine mesh of thin parallel wires. The orientation within a domain is such that the effective mesh of wires runs at right angles to those in neighbouring domains. This suggests that the domains act rather like a wire grid polariser and that absorption of the light will be strongest for those components of the electric vector that lie parallel to the grid structure. This specimen may therefore be regarded as dichroic with uniform dichroism within a domain but with a 90° rotation of orientation between domains. We show in Fig. 5(a) and (b) the raw demodulated quadrature 'sin' and 'cos' images, together with the information, orientation, Fig. 5(c) and magnitude, Fig. 5(d), which can be extracted. A helium neon laser was used as the light source together with a 0.85 numerical aperture objective lens. We also show a colour coded image which combines all the polarization contrast information into one image, Fig. 5(e), where we have used the colour code of Fig. 4. We see that the orientation changes by 90° between domains as predicted, and that the magnitude of the dichroism is essentially constant within a domain. Our system is, of course, also capable of providing a reflected light confocal image. The only information that can be gained from this image, Fig. 5(f), is the presence of a crack running diagonally across the field of view; nothing can be inferred about the non-uniform domain structure. This can only be seen in the polarization contrast images. Figure 6 further emphasizes this point by showing an image using an alternate method of presenting the data. In this representation the length of the line represents the magnitude of the dichroism and the direction of the line coincides with the orientation.

Fig. 4. The colour map used to encode the state of polarization of the light reflected from the sample. The direction of the arrow denotes the orientation of the principal axis of the ellipse via the hue of the colour, whereas the saturation, radial distance, encodes the ellipticity. The centre of the circle corresponds to unit ellipticity (circular polarization), whereas the edge denotes minimum ellipticity present in the image. The same colour-coding scheme is used in all the figures.

A further example is shown in Fig. 7 of a Smectic C* liquid crystal, which shows strong birefringent properties due to the orientation of the directors, which are sensitive to surface alignment. Changes in the orientation of the directors are reflected in the change of colour. Using the colour map to interpret these changes reveals that the difference in angle between the yellow and blue areas is quite significant. Again, hardly any of these details are visible in the reflection image.

The images we have just shown were of specimens which were inherently optically anisotropic. However, polarization contrast also arises due to scattering from specimen features. As an example of this we show in Fig. 8 polarization images of a single scale from a butterfly's wing. In the lower magnification image we see a predominantly longitudinal structure, whereas the higher magnification image reveals a finer transverse structure. The source of image contrast in this case is the polarization-dependent scattering of light from the essentially diffraction grating-like structure of the wing. This form of polarization contrast is further illustrated in Fig. 9, where we show the polarization contrast image of a cleaved edge of a semiconductor. In this case, edge scattering is the source of image contrast, as can be seen by the orientation of the diffracted

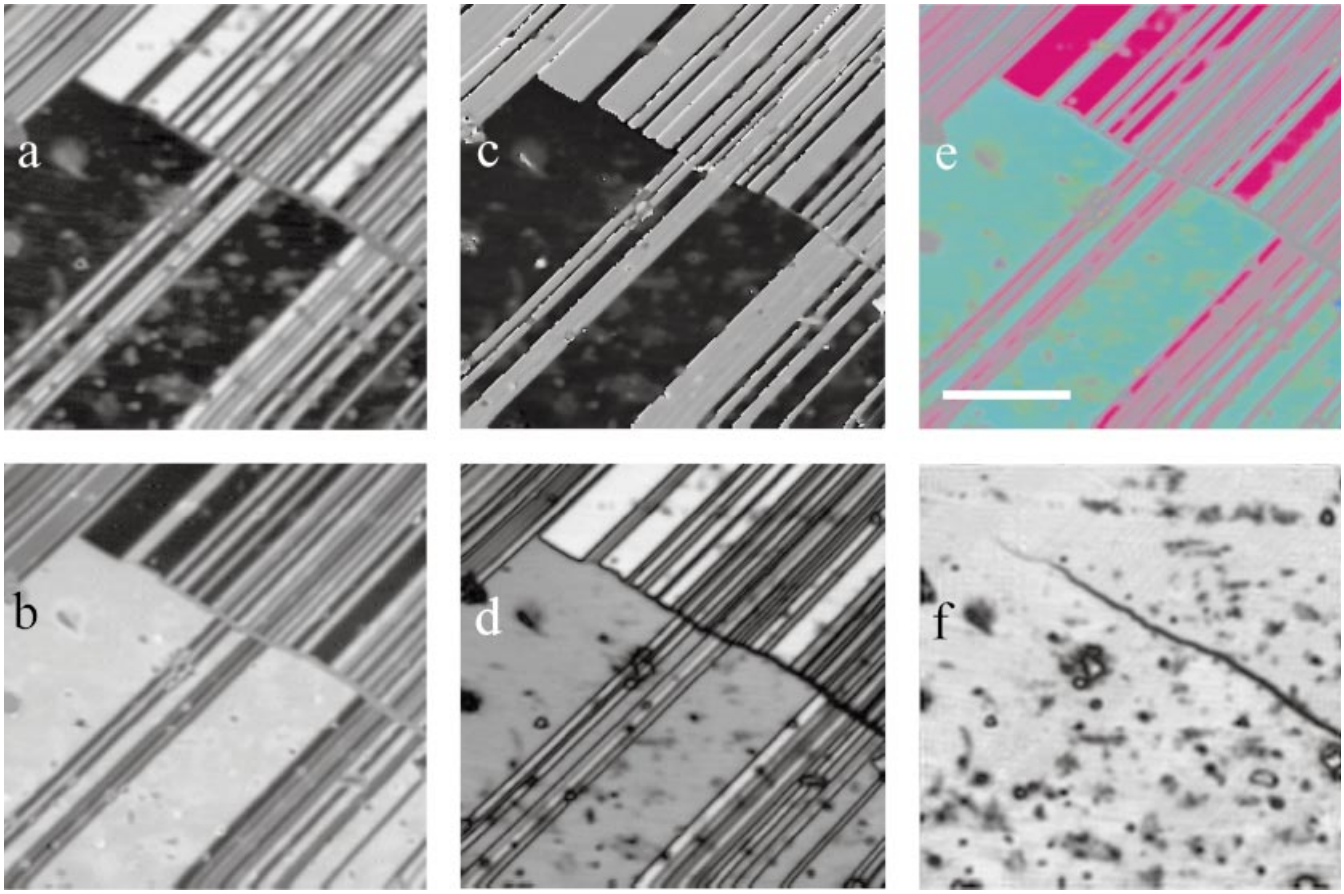

Fig. 5. Images of a section of the superconducting crystal $Y_1Ba_2Cu_3O_{6.94}$. (a) and (b) show the two quadrature demodulated signals from the lock-in detector from which the orientation (c) and magnitude (d) images are derived. These two images may be combined into a single colour-coded polarization contrast image (e) using the colour mapping of Fig. 4. Finally, a reflected light confocal image (f) is presented. The scale bar represents 5 μm.

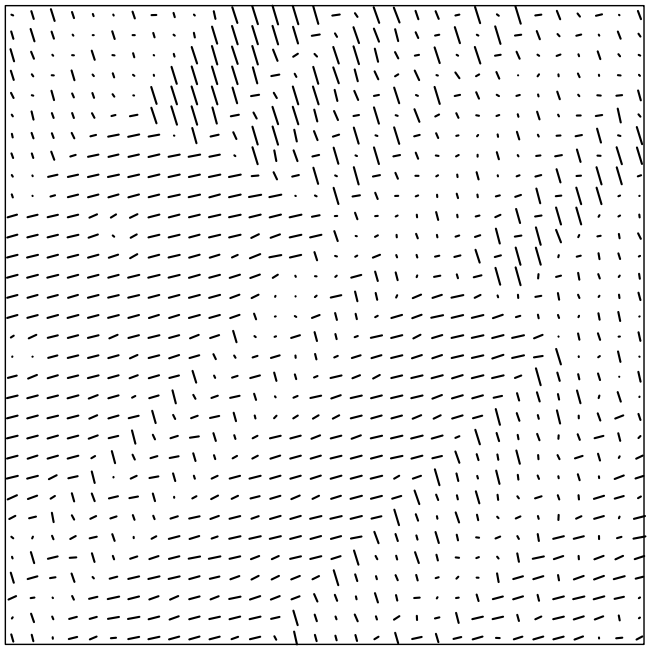

field. We also see that the dark spots of dirt on the semiconductor in the reflected light image appear to be imaged in a complicated way in the polarization contrast image. Because the features in this case are simply examples of point-like objects, and hence likely to appear in one form or another in a variety of specimens, we now discuss in detail how these objects are imaged in the polarization contrast microscope.

In order to model the image contrast observed when imaging specimens containing point scatterers, we assume that such features act as radiating dipoles the dipole moment of which is proportional to the incident electric field. The details of the theoretical considerations are described in the Appendix, where it is assumed that the scatterer is positioned on a highly reflecting substrate. For the case when the microscope is focused on the scatterer the functions I_0, I_1 and I_2 are seen to be

Fig. 6. Image of the same region of the superconducting crystal $Y_1Ba_2Cu_3O_{6.94}$ as Fig. 5. In this image lines are used to represent the polarization contrast; the length of the line indicates the magnitude of the anisotropy, whereas the angle corresponds to the orientation.

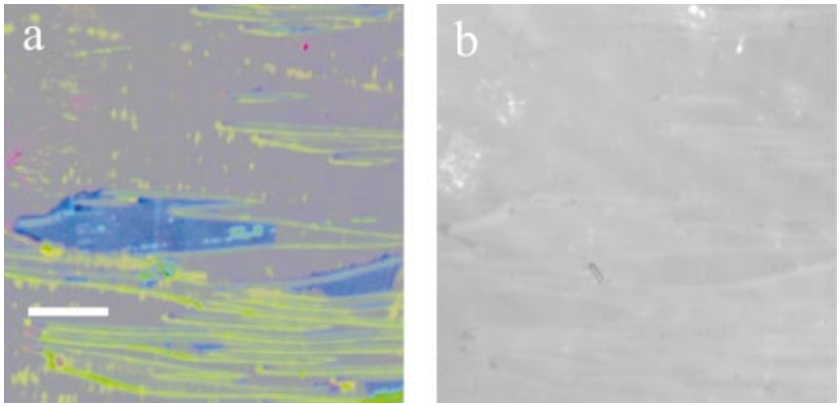

Fig. 7. Polarization (a) and confocal reflected light (b) images a Smectic C* ferroelectric liquid crystal. The scale bar represents 10 μm.

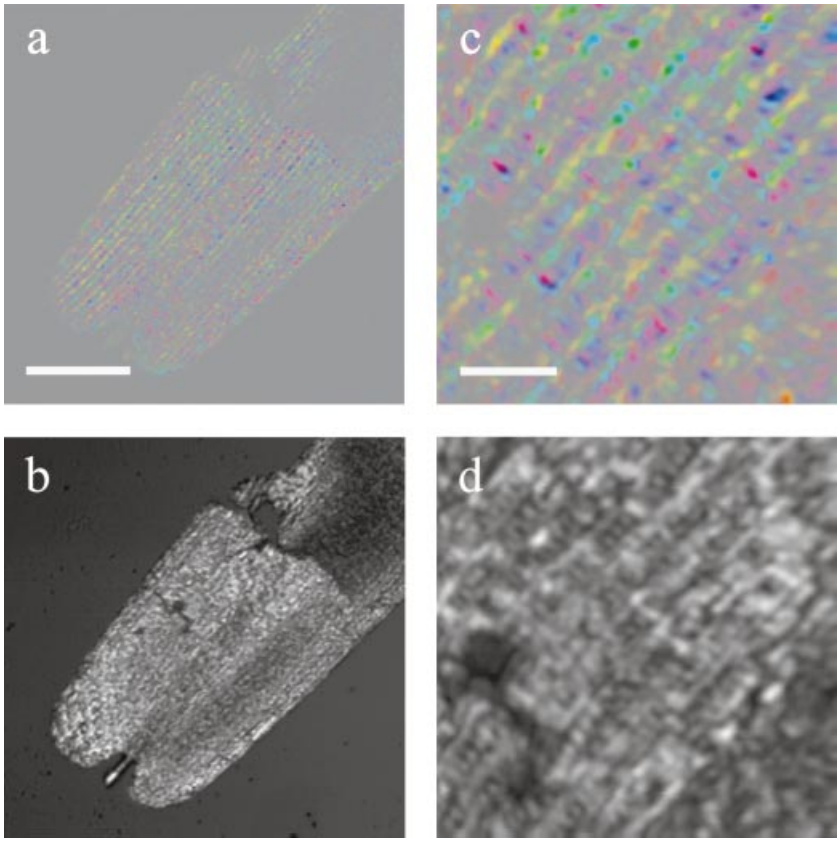

Fig. 8. A single scale of a butterfly wing. The polarization and reflection images are shown in (a) and (b), where the scale bar represents 25 μm, and again, at higher magnification in (c) and (d), where the scale bar now represents 5 μm.

real and hence the demodulated quadrature images are given, from Eqs (A4) and (A5), by:

$$I_c \sim (I_1^2 + I_0 I_2)\cos(2\phi_s) \tag{19}$$

and

$$I_s \sim (I_1^2 + I_0 I_2)\sin(2\phi_s) \tag{20}$$

where ϕ_s is the angular polar co-ordinate. The lock-in detector extracts the phase, $2\phi_s$, which therefore varies from 0 to 4π. Figure 10 shows the form of these demodulated functions as well as the individual magnitude and orientation images. In all cases, the theoretical predictions are confirmed experimentally as shown. Finally, we also show, in Fig. 10, the combined magnitude and orientation image as a single colour-coded polarization contrast image. The similarity between this image and that of the point defect in Fig. 9 is striking.

We finally show, in Fig. 11, the effects of defocus. In this case, the simplified expressions of Eqs (19) and (20) are no longer valid and it is necessary to use the full expressions in the Appendix. The figure concentrates on the demodulated

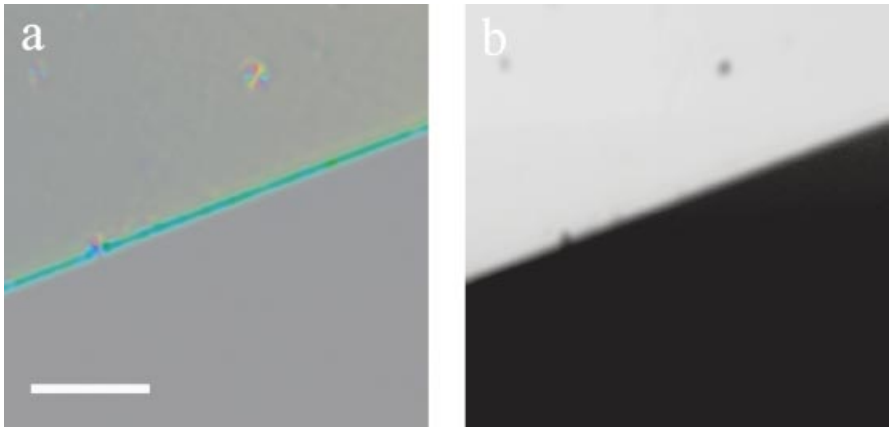

Fig. 9. Polarization (a) and reflected light confocal (b) images of a cleaved edge of indium phosphide. The images show both the effects of edge scattering as well as the polarization images to be expected from a point scatterer. The scale bar represents 5 μm.

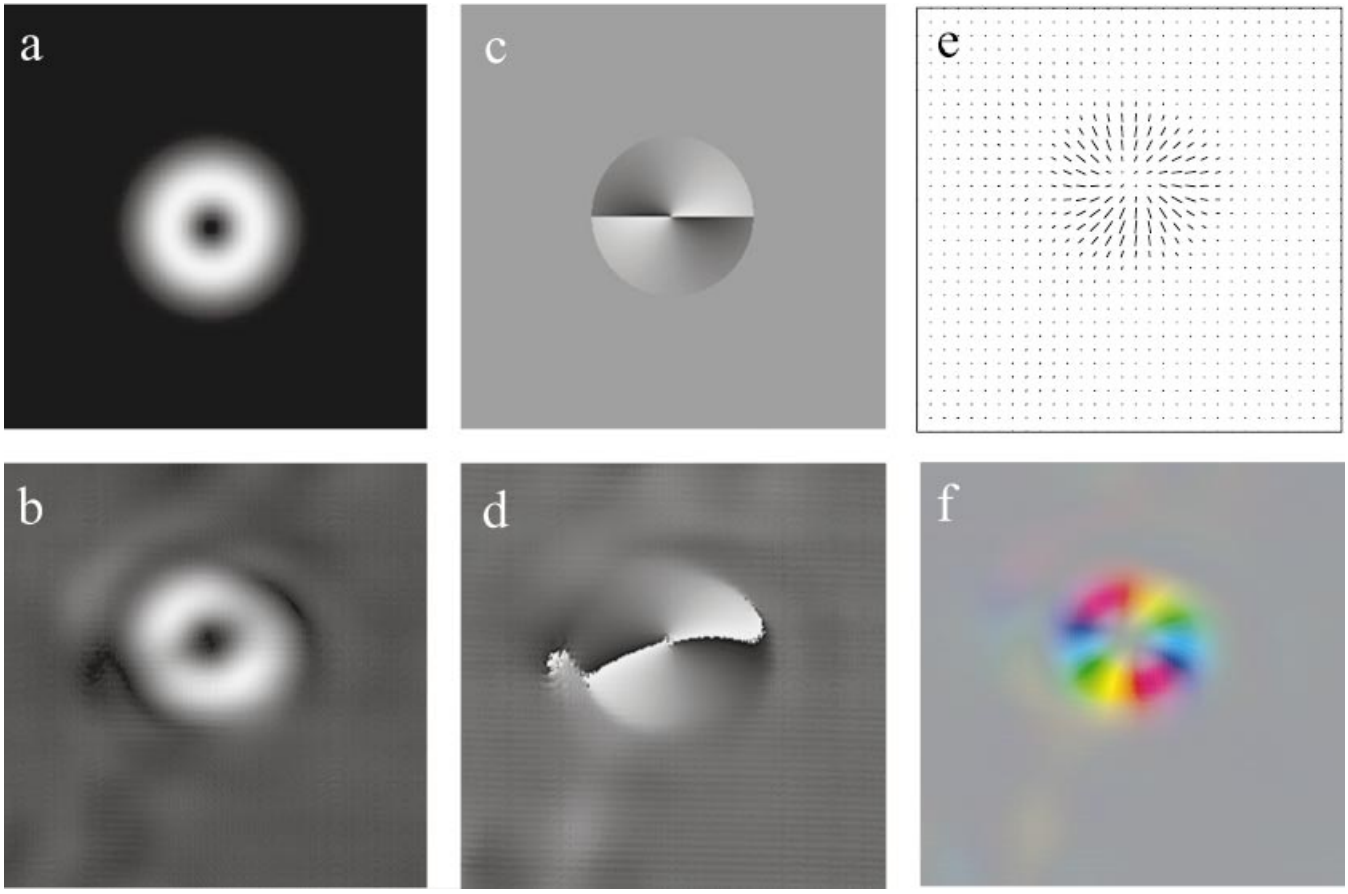

Fig. 10. A comparison between theory and experiment in the imaging of a point scatterer. (a) and (c) show the theoretically predicted magnitude and orientation images together with the experimental confirmation in (b) and (d), respectively. Combined experimental polarization images are shown in (e) and (f) using the two alternative representations previously introduced.

signal in the in-focus and defocus cases both theoretically and experimentally. The spiral shape exhibited in the defocus case is a feature commonly encountered and it is important to realize that this contrast arises from defocus and not from some inherent birefringent property of the specimen. As in the case of the edge (Fig. 9), the contrast is due to the three-dimensional vectorial nature of the focused light beam and not to any instrinsic material birefringence.

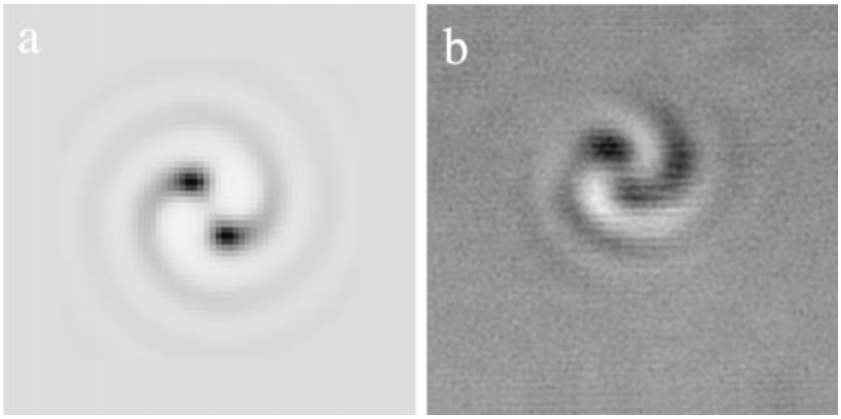

Fig. 11. The effect of defocus is illustrated by comparing the theoretical (a) and experimental (b) demodulated images for a defocus value corresponding to $kz = 5$.

Conclusions

We have described a simple method whereby a confocal microscope may be modified so as to give additional information about the optical anisotropy of the specimen. The modification, which does not compromise the image acquisition speed, permits additional images to be obtained where contrast relates, in the case of a birefringent specimen, to both orientation and retardance. We have discussed the origin of image contrast and have shown that valuable information may be extracted from these images, which is completely absent in conventional bright-field imaging. Further, the origin of the contrast observed in the polarization contrast images in isotropic point scatterers has been identified and theoretically modelled.

References

Azzam, R.M.A. & Bashara, N.M. (1989) *Ellipsometry and Polarised Light.* North Holland, Amsterdam.

Born, M. & Wolf, E. (1975) *Principles of Optics*. Pergamon, Oxford.

Gay, P. (1967) *An Introduction to Crystal Optics*. Longman, London.

Glazer, A.M., Lewis, J.G. & Kaminsky, W. (1996) An automatic optical imaging system for imaging birefringent media. *Proc. Roy. Soc. London A*, **452**, 2751–2765.

Inoué, S. (1986) *Video Microscopy*. Plenum, New York.

Kubota, H. & Inoué, S. (1959) Diffraction images in the polarising microscope. *J. Opt. Soc. Am.* **49**, 191–198.

Oldenbourg, R. & Mei, G. (1995) New polarised light microscope with precision universal compensator. *J. Microsc.* **180**, 140–147.

Pluta, M. (1993) *Advanced Light Microscopy, Vol. 3. Measuring Techniques.* Elsevier, Amsterdam.

Richards, B. & Wolf, E. (1959) Electromagnetic diffraction in optical systems. II. Structure of the image field in an aplanatic system. *Proc. Roy. Soc. A*, **253**, 358.

Robinson, P.C. & Bradbury, S. (1992) *Qualitative Polarised Light Microscopy*. Oxford University Press, Oxford.

Wilson, T., ed. (1990) *Confocal Microscopy*. Academic Press, London.

Wilson, T. & Juškaitis, R. (1995) On the extinction coefficient in confocal polarization microscopy. *J. Microsc.* **179**, 238–240.

Wilson, T., Jukaitis, R. & Higdon, P.D. (1997) The imaging of dielectric point scatterers in conventional and confocal polarisation microscopes. *Optics Comm.* **141**, 298–313.

Wilson, T. & Sheppard, C.J.R. (1984) *Theory and Practice of Scanning Optical Microscopy*. Academic Press, London.

Appendix

In order to model the polarization contrast seen when imaging specimens containing subresolution point scatterers, we elect to regard such features as radiating dipoles the dipole moment of which is proportional to the incident electric field. This is an approach that has been used elsewhere and has been found to predict accurately the image contrast seen with such objects in standard confocal and conventional microscopes (Wilson *et al.*, 1997). We model the incident field at the focus of a high numerical aperture microscope objective using the theory of Richards & Wolf *et al.* (1959) and then propagate the scattered far-field through the optical system to the confocal point detector. The calculation is a straightforward extension of that reported earlier (Wilson *et al.*, 1997). Therefore, we will do no more here than write the result for the confocal amplitude image signal, with circularly polarized illumination, when it is detected through an analyser orientated at an angle $\gamma(\omega t/2)$ to the x-axis.

$$U = \frac{e^{j\phi_s}}{\sqrt{2}}\left\{(I_0^2 + I_2^2 + 2I_1^2)\,e^{-j(\phi_s-\omega t/2)} + 2(I_1^2 + I_0 I_2)\,e^{j(\phi_s-\omega t/2)}\right\} \quad \text{(A1)}$$

and the functions $I_{0,1,2}$ are given by Richards & Wolf (1959):

$$I_0(\nu,\alpha) = \int_0^\alpha \cos^{\frac{1}{2}}\theta \sin\theta\,(1+\cos\theta)\,J_0\left(\frac{\nu\sin\theta}{\sin\alpha}\right)\exp(jkz\cos\theta)\,d\theta$$

$$I_1(\nu,\alpha) = \int_0^\alpha \cos^{\frac{1}{2}}\theta \sin^2\theta\,J_1\left(\frac{\nu\sin\theta}{\sin\alpha}\right)\exp(jkz\cos\theta)\,d\theta$$

$$I_2(\nu,\alpha) = \int_0^\alpha \cos^{\frac{1}{2}}\theta \sin\theta\,(1-\cos\theta)\,J_2\left(\frac{\nu\sin\theta}{\sin\alpha}\right)\exp(jkz\cos\theta)\,d\theta \quad \text{(A2)}$$

where the angle α denotes the angular aperture of the objective lens, z the defocus value and $J_0(.)$, $J_1(.)$ and $J_2(.)$ represent zero-, first- and second-order Bessel functions of the first kind, respectively. The polar co-ordinates of the scan are denoted by ρ_s and ϕ_s. The co-ordinate v is the optical co-ordinate corresponding to the scan distance in the object plane ($v = k \rho_s \sin \alpha$).

In our experiments, however, the point scatterers are sitting on a planar reflecting substrate, which leads to an additional confocal image field of the form

$$R\begin{pmatrix}1\\ j\end{pmatrix}$$

where the reflectivity R of the substrate makes a considerably greater contribution to the total image signal level than the subresolution point scatter. The final detected image intensity is given by:

$$I = |U + \mathrm{Re}^{j\omega t/2}|^2 \tag{A3}$$

Synchronous demodulation of the image intensity, for the case where the reflected field R is considerably stronger than the field from the point scatterer, then gives the following quadrature components result:

$$I_c \sim \mathrm{Re}\left\{(I_1^2 + I_0 I_2)e^{2j\phi_s}\right\} \tag{A4}$$

and

$$I_s \sim \mathrm{Im}\left\{(I_1^2 + I_0 I_2)e^{2j\phi_s}\right\} \tag{A5}$$

which gives an image corresponding to the magnitude of the form $|I_1^2 + I_0 I_2|$, which is seen to be zero when $v = 0$, when the point scatterer is located on the optic axis. The argument, by contrast, is given by $2\phi_s$, which therefore undergoes a 4π variation.